

Black hole binaries in shift-symmetric Einstein-scalar-Gauss-Bonnet gravity experience a slower merger phase

Maxence Corman,^{1,*} Llibert Aresté Saló,^{2,3,†} and Katy Clough^{4,‡}

¹*Max Planck Institute for Gravitational Physics (Albert Einstein Institute), D-14476 Potsdam, Germany*

²*Instituut voor Theoretische Fysica, KU Leuven. Celestijnenlaan 200D, B-3001 Leuven, Belgium.*

³*Leuven Gravity Institute, KU Leuven. Celestijnenlaan 200D, B-3001 Leuven, Belgium.*

⁴*School of Mathematical Sciences, Queen Mary University of London,
Mile End Road, London, E1 4NS, United Kingdom*

In shift-symmetric Einstein-scalar-Gauss-Bonnet gravity, stationary black holes have a non-vanishing scalar charge. During the inspiral, the phase evolution is modified by several effects, primarily an additional scalar dipole radiation, which enters at -1PN order. This effect accelerates the inspiral when compared to general relativity, when including corrections up to 2PN. Using fully non-linear numerical simulations of quasi-circular, comparable mass binaries, we find that in the late stages the orbital dynamics are altered so that the overall effect is instead a decelerated merger phase for the modified gravity case. We attribute this to a change in the conservative dynamics, and show that at the late inspiral stage more energy must be emitted in scalar-Gauss-Bonnet gravity to induce a given change in frequency. In longer signals, this should lead to a distinctive switch between a faster and slower frequency evolution relative to general relativity as the binary approaches merger. This work suggests we should revisit existing constraints on the theory that are obtained assuming PN approximations apply up to merger, or based on order by order approximations that neglect backreaction effects on the metric, and shows the importance of including non-linear effects that modify the gravitational sector in the strong field regime.

Introduction.— Gravitational waves (GWs) from compact binary coalescences provide a unique probe of the strong field regime of black holes (BHs) [1–3]. Observations by the LIGO-Virgo-KAGRA network of detectors are currently ongoing [4, 5], and the future proposed detectors LISA [6], the Einstein Telescope [7, 8], and Cosmic Explorer [9] will provide a significant upgrade in the precision that can be achieved. These messengers carry information about a previously unexplored regime of parameter space, probing stronger potentials and higher curvatures than previous observations [10], and therefore, there is a possibility that new effects from high-energy corrections to general relativity (GR) may be observed.

Based on the data we have to date, any deviations are expected to be small [11–16]. Effective Field Theories (EFTs) of gravity therefore provide a well-motivated way to organize and constrain corrections to GR. A given EFT specifies any lower energy degrees of freedom and symmetries that should be respected, and then parametrizes the leading order terms in the action that modify GR in powers of a dimensionful coupling λ that is small at the relevant curvature scale (e.g. for the binary, this scale is set by the inverse of the Schwarzschild radius). Constraints on the coupling can then be translated into bounds on possible UV completions and their properties (see e.g. [17–20]).

Einstein-scalar-Gauss-Bonnet (EsGB) gravity considers the effect of an additional scalar degree of freedom, which couples to the Gauss-Bonnet invariant via an arbitrary coupling function which can be expressed from an EFT point of view as a power expansion of the scalar. In the shift-symmetric case, this function is linear, which rep-

resents the leading order parity-invariant correction to GR for a scalar-tensor theory of gravity in the vacuum theory [21]. In such a theory, the scalar is sourced by spacetime curvature and all BHs should carry a scalar charge [22–24]. As a result, the theory is relatively well constrained by observations, but tests so far rely mainly on Post-Newtonian (PN) approximations [25–27] that cannot capture the fully non-linear regime near merger, or order-reduced approximations that are known to suffer from spurious secular growth [28]. Consequently, there has been a significant effort to develop fully non-linear simulations of binaries in this and other beyond-GR theories using numerical relativity (NR) to generate more accurate waveforms.

The key test is whether the correct waveforms are distinguishable from GR signals when injected into the data-stream. It is possible that, whilst they may differ, the beyond-GR effects simply change the measurement of the intrinsic binary parameters. If the residual, once the best fit GR waveform is subtracted, is small, it may not be significant enough to trigger a detection with current detector sensitivities. This could be the case where, for example, there is a simple overall increase in the rate of dephasing, which could be mimicked by larger BH masses.

A major breakthrough enabling the construction of injectable signals was the demonstration by Kovács and Reall that some higher-derivative scalar-tensor theories admit a well-posed initial value formulation in the weakly coupled regime when expressed in modified generalized harmonic (MGH) coordinates [29, 30]. This formulation, and a variation of it developed later for puncture based codes using a modified CCZ4 formalism (mCCZ4) [31, 32],

permitted the first fully non-linear evolutions in such theories [33], followed later by others [34–41], and enabled the quantification of error in alternative methods [42], such as the order by order approach [43–48] and the hydrodynamics inspired “fixing the equations” technique [49–53]. Initial simulations mainly focused on the tendency of evolutions to remain in the weakly coupled regime in which the EFT is valid in dynamical strong field cases [34, 37, 54] and proof of principle studies of binary evolutions [32–35]. More recent works have attempted to render the simulations more precise, but have encountered difficulties in controlling the initial data and eccentricity, as well as quantifying the small effects that arise due to numerical errors [36, 41]. Improvements to the techniques that would enhance the quality of initial data are being developed [55, 56], but the problem remains challenging.

In this Letter, we present carefully calibrated simulations for a binary with intrinsic parameters similar to the first detected GW event, GW150914 [57], and compare the GR and EsGB waveforms. These results indicate that the modified theory exhibits a deceleration in the phase evolution during the late inspiral phase, leading to a delayed merger, as shown in Fig. 1. This challenges the conventional expectation that an additional scalar degree of freedom leads to a faster inspiral, and may require constraints on the theory to be revised. We verify this result using the two independent codes that have implemented the MGH and mCCZ4 formulations of the equations, and identify the cause as a change in the conservative dynamics, where more energy must be emitted in the modified theory to induce a given change in the frequency. Although our waveforms are too short to identify the point of transition, we still expect the early inspiral to be dominated by the dissipative effects of the scalar radiation, and therefore for the phase evolution to be accelerated relative to GR for the same intrinsic parameters. This transition relative to GR - first faster, then slower - from inspiral to merger, should be more distinctive from an observational perspective than dephasing in a single direction.

We use geometric units: $G = c = 1$, the metric convention $- + + +$, and lower case Latin letters to index space-time indices. The Riemann tensor is $R^a_{bcd} = \partial_c \Gamma^a_{db} - \dots$.

EsGB theory.— We consider shift-symmetric EsGB gravity, which has an action given by

$$S = \frac{1}{16\pi} \int d^4x \sqrt{-g} \left(R - (\nabla\phi)^2 + 2\lambda\phi\mathcal{G} \right), \quad (1)$$

where g is the determinant of the spacetime metric and \mathcal{G} is the Gauss-Bonnet scalar given by $\mathcal{G} \equiv R^2 - 4R_{ab}R^{ab} + R_{abcd}R^{abcd}$. Here, λ is a constant coupling parameter that, in geometric units, has dimensions of length squared. As the Gauss-Bonnet scalar \mathcal{G} is a total derivative in four dimensions, we see that the action is preserved up to total derivatives under constant shifts in the scalar field:

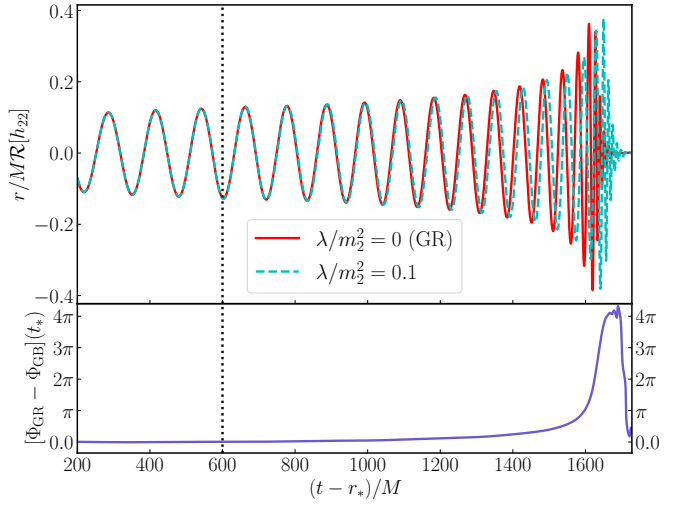


FIG. 1. Here we show the strain waveform for EsGB and GR for the intrinsic parameters of a GW150914-like event using the mCCZ4 formulation. The signals have been aligned in frequency and phase according to (4)–(5) over time window ranging from $t_i = 200M$ to $t_f = 600M$, the latter shown by the vertical dotted line. One can see that the GR waveform merges *earlier* than the EsGB case, contrary to the naive expectation that the extra scalar radiation channel will result in a faster merger. The bottom panel shows the dephasing as a function of retarded time $t_* \equiv (t - r_*)/M$.

$\phi \rightarrow \phi + \text{constant}$. Schwarzschild and Kerr BHs are not stationary solutions in this theory: if one begins with such vacuum initial data, the BHs will dynamically develop stable scalar clouds (hair). The end state is a BH with non-zero scalar charge Q_{SF} , such that at large radius the scalar field falls off like $\phi = \phi_0 + Q_{SF}/r + \mathcal{O}(1/r^2)$, ϕ_0 being the scalar field value at spatial infinity imposed by the binary’s cosmological environment. Studies have found that stationary solutions exist, as long as the coupling normalized by the total BH mass as measured at infinity m , λ/m^2 , is sufficiently small [23, 24, 33, 58, 59]. One expects BH binaries to emit scalar radiation, thus increasing the inspiral rate of binaries [60, 61]. The most stringent observational bound on the theory comes from comparing the black hole-neutron star GW signal GW230529 to Post-Newtonian results for EsGB and give a constraint of (after restoring dimensions) $\sqrt{\lambda} \lesssim 0.63$ km [27].

The covariant equations of motion for shift-symmetric EsGB gravity are

$$\square\phi + \lambda\mathcal{G} = 0, \quad (2)$$

$$R_{ab} - \frac{1}{2}g_{ab}R - \nabla_a\phi\nabla_b\phi + \frac{1}{2}(\nabla\phi)^2g_{ab} + 2\lambda\delta_{ijg(a}^{efcd}g_{b)d}R^{ij}{}_{ef}\nabla^g\nabla_c\phi = 0, \quad (3)$$

where δ_{efgh}^{abcd} is the generalized Kronecker delta tensor.

Formulation and methods.— To study the full, non-perturbative, shift-symmetric EsGB equations, we em-

ploy two independent formulations of the Einstein equations, each with its own numerical implementation: the MGH formulation [29, 30] used in [33], and the modified CCZ4 (mCCZ4) formulation [31, 32] implemented in `GRFolres` [62] as an extension to `GRChombo` [63, 64]. Both formulations introduce two auxiliary Lorentzian metrics to fix the gauge, high-order finite differencing with Runge–Kutta time integration, and adaptive mesh refinement, but they differ in important aspects. The MGH scheme evolves the covariant system directly in compactified coordinates with a modified version of the damped harmonic gauge and relies on dynamic excision of regions within apparent horizons, whereas the mCCZ4 approach uses a 3+1 conformal decomposition on a finite Cartesian grid with moving-puncture gauge conditions. A detailed comparison of the formulations and numerical methods is provided in the Supplemental Material (SM).

For initial data, we do not implement a method to solve for the Hamiltonian and momentum constraint equations for general ϕ , but instead choose $\phi = \partial_t \phi = 0$, in which case the constraint equations of EsGB are the same as in GR (see Ref. [33]). We thus consider binary vacuum GR BH solutions, constructed using the BH puncture method with the `TwoPunctures` [65–67] code. For the scalar field, we slowly ramp up the coupling of the theory as described in Appendix B of Ref. [68] over a period of time (typically $\sim 150M$, with M the total ADM mass of the spacetime). We study a system with parameters consistent with GW150914 [69], specifically, those used in Fig. 1 of the GW150914 detection paper [57]. We set the spins to zero and the mass ratio to $q = 1.221$, giving initial puncture mass values of $m_1 = 0.5497M$ and $m_2 = 0.4502M$. We choose an initial separation of $11.8M$ such that, in GR, the BHs merge after ~ 9 orbits (roughly $1700M$). We consider a coupling value of $\lambda/m_2^2 = 0.1$, which, assuming the smallest BH observed so far is $3.6M_\odot$, corresponds to ~ 1.7 km, i.e. larger by a factor of ~ 2 than the current bounds we have on this theory. Though these bounds rely on the assumption that PN theory is valid up to merger, which, as we show here, may not be valid. We estimate the initial orbital eccentricity of our GR runs to be $\sim 10^{-3}$. Without any adjustment of the parameters, the $\lambda/m_2^2 = 0.1$ runs result in initial orbital eccentricities of $\sim 10^{-2}$ due to being perturbed by the development of the scalar field around the BHs at early times, which is an artefact of the initial conditions we use. In previous studies [36, 38, 41, 42] we had found that residual eccentricity from the initial data was subdominant to finite-resolution truncation errors, because the energy contained in the scalar cloud, for the couplings and initial separations we considered, was only a small fraction of the total binary binding energy. However this is no longer true for the larger initial separation and coupling values we consider in this work. Therefore, we perform eccentricity reduction following the methods of [70, 71] and reduce the eccentricities to $\sim 2 \times 10^{-3}$ and

$\sim 3 \times 10^{-3}$ for the MGH and mCCZ4 codes respectively.

We use many of the same diagnostics introduced in Refs. [33, 36]. We measure the scalar and gravitational radiation by extracting the Newman-Penrose scalar Ψ_4 and scalar field ϕ on coordinate spheres at large radii (typically $r = 100M$) and decomposing these quantities into spin -2 and 0 weighted spherical harmonics. We use Ψ_4 to calculate an associated gravitational wave luminosity P_{GW} and ϕ to measure the flux of energy in the scalar field P_{SF} (cf. Eq. (6) and Eq. (9) in [36]). We neglect effects due to slightly different gauges/physical extraction radii at this time [72]; at such distances, their effect would be significantly smaller than the measured physical waveforms. We also verified that extrapolating our waveforms at infinity does not affect the phase and only slightly changes the amplitude, so considering finite radii is sufficient for the purposes of this work.

We calculate the gravitational wave strain $h \equiv h_+ + ih_\times$, related to Ψ_4 through $\Psi_4 = \ddot{h}$ using fixed frequency integration [73]. We further decompose the $h_{22}(t)$ mode into a real time-domain amplitude $A(t)$ and phase $\Phi(t)$ as $h_{22}(t) = A(t)e^{-i\Phi(t)}$ giving a GW frequency (assuming the stationary phase approximation) $\omega(t) = 2\pi f(t) = \frac{d}{dt}\Phi(t)$. During the evolution, we track any apparent horizons (AH) present at a given time, and measure their corresponding areas \mathcal{A}_{H} . From this, we compute a measure of the BH mass M_{H} via the Christodoulou formula [74] - see further comments on this below.

Definition of dephasing and mass in different theories.— Taking the view of an observer far from the binary measuring the signal, we see a wave with an initial frequency f_1 and follow it up to a frequency f_2 (or merger). Say we observe n cycles in GR. If EsGB modifies the binary evolution, we expect to measure a different number of cycles in this frequency interval. This tells us that the rate of inspiral has changed. But to compare the two systems meaningfully in this way, we should fix the intrinsic binary parameters to be the same in both cases. Our finding therefore rests in part on the definition of “like-for-like” intrinsic parameters in GR versus EsGB. Since the systems are physically different, and evolve dynamically in different ways, it is not clear that there is a unique way to compare them. However, having fixed the spins to be zero and reduced the initial eccentricities to be roughly zero, the problem reduces to the question of what we mean by equivalent masses. From an NR perspective the only gauge invariant notion of the mass of the spacetime is given by the total ADM mass M_{ADM} , so in our simulations we fix this to be the same in both cases in the initial data. This also fixes the units of time of the asymptotic observer – in the asymptotic region, the scalar field value is negligible and we are essentially in GR - here Newton’s constant $G = 1$ controls the mapping between energy/mass and time/length, so units are the same in GR and EsGB for a fixed M_{ADM} (see the SM for a

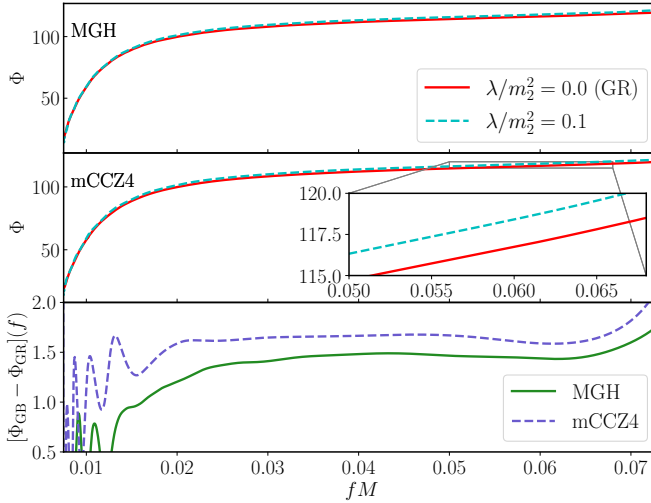


FIG. 2. In this figure we show the phase evolution versus frequency, using the same alignment as Fig. 1. In the top panel we show the phase Φ versus frequency f between GR and EsGB for the mCCZ4 code, and in the second for the MGH code. In the final panel only the difference to GR is plotted for both codes, which is the most robust comparison. Whilst the effect is small, the two show a clear consistency in predicting a slower inspiral in EsGB after alignment (seen here as more cycles accumulating in EsGB for a given change in frequency).

detailed discussion about the ADM mass of the spacetime and how it relates to the notion of ADM mass used in PN calculations). However, note that in the EsGB case this means that after the initial transient scalarization, some of the mass energy will be in the scalar charge, and the quasi-local masses associated with the horizon areas of the BHs via the Christodoulou formula will be smaller. The presence of a scalar charge also means that a given observed frequency will correspond to a different orbital separation (loosely speaking, since separation is gauge dependent in the strong field regime), as the local effective strength of gravity is modified.

Results.— Our main result is shown in Fig. 1, where we compare the strains for the GR and EsGB cases as a function of time after aligning them in frequency and phase over an initial time interval, and observe an earlier merger in the GR case. We see that the EsGB binary is spiralling in more slowly - $df/dt = d^2\Phi/dt^2$ is *smaller*, such that after the alignment (which sets the initial phase and its first time derivative equal) $\Phi_{\text{GR}}(t_*) > \Phi_{\text{GB}}(t_*)$ at any given retarded time, $t_* \equiv (t - r_*)/M$. In Fig. 2 we instead show the dephasing as a function of frequency and find that $\Phi_{\text{GB}}(f) > \Phi_{\text{GR}}(f)$ at any given frequency, meaning that the EsGB waveform has to go through more cycles than in GR to reach a given frequency. Note that at a fixed frequency $d\Phi/df \sim (df/dt)^{-1}$, which explains the opposite sign of the phase difference compared to the time dependence shown in Fig. 1. This is opposite to what one

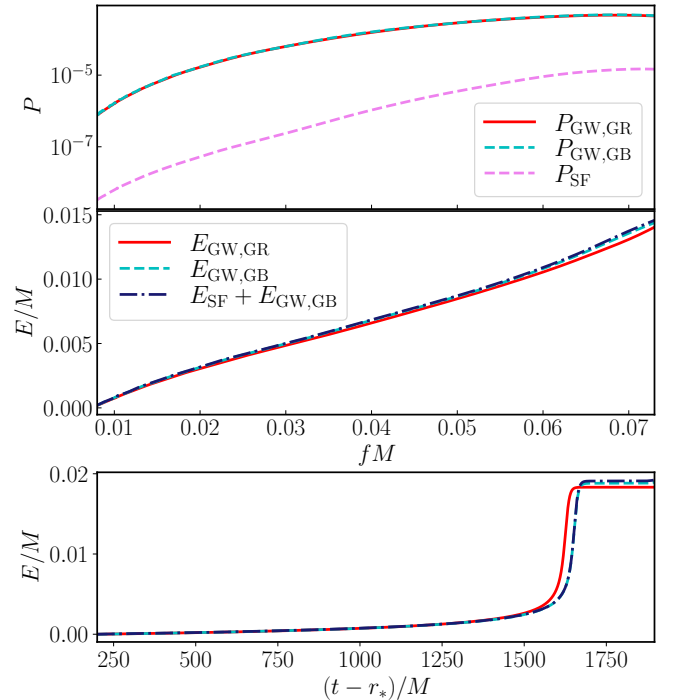


FIG. 3. We plot the GW $P_{\text{GW}} = dE_{\text{GW}}/dt$ and scalar P_{SF} luminosity versus frequency. We see that the GW radiation appears to be roughly consistent between GR and EsGB at a given frequency, while the scalar radiation is orders of magnitude smaller. However, in the second panel we plot the integrated GW luminosity vs the frequency and find that in the approach to merger this is smaller in GR than in EsGB, implying a modification in the binding energy at a given frequency, which is what leads to the delayed merger. In the bottom panel we plot the integrated GW luminosity versus retarded time for EsGB and GR. It can be seen that the end value is smaller for GR - less emission was needed to reach merger than in EsGB.

would naively expect from PN calculations. The bottom panel of Fig. 2 also shows that the observed dephasing is highly consistent between the two independent codes, which gives us confidence that this result is not due to code or numerical errors. Although we find differences between the two codes in the specific values that are sometimes comparable to the differences between GR and EsGB, this is not unexpected given the many differences detailed above, which means that they are likely to experience different initial transients and sources of truncation error. However, the dephasing between GR and EsGB for both codes (which tends to depend less on things like code-specific truncation errors [36]) are highly consistent. In the SM we provide further details on the comparison and validation of our codes, including robustness studies for the alignment method used. We also discuss what PN calculations predict for this system, subtleties in the definition of the ADM mass and why this effect was not seen in past works.

To understand the origin of the dephasing better, in Fig. 3, we consider the evolution of several quantities with respect to frequency and time. In the top panel we plot the GW luminosity $P_{\text{GW}} = dE_{\text{GW}}/dt$ as a function of frequency f , which is found to be very similar between GR and EsGB. The flux of energy in the scalar field, P_{SF} , is subdominant by two orders of magnitude, meaning we are in the so-called *quadrupolar driven regime* [75]. In general the quadrupole radiation should depend non-trivially on the values and gradients of the scalar at the late inspiral/merger stage, and it is therefore not obvious that the power as a function of frequency should remain unchanged, but it appears to be the case here. Given that $df/dt \sim P df/dE$, we therefore conclude that the observed deceleration of the EsGB merger (smaller df/dt) is the result of a smaller change in frequency with a given emission of energy, and this is verified in the second panel (dE/df is larger for EsGB). The third panel displays the total energy emission in the time domain, demonstrating that a higher value is emitted following alignment in order to reach merger in the EsGB case. We also find that the ADM mass of remnant is smaller by $\sim 1\%$. In summary, these results suggest that modifications to the metric due to the presence of the scalar have changed the binding energy of orbits corresponding to given frequencies. More energy now needs to be emitted for the orbital frequency to increase by a given amount in the modified theory, which, given that the radiation power remains roughly comparable, means that it proceeds at a slower rate.

Discussion.— Studying the dynamical and non-linear regime of modified theories of gravity remains a major theoretical challenge, limiting our ability to place the most stringent constraints on these models. In recent years, several groups have independently solved the full equations of motion for a broad class of modified theories of gravity. Numerical codes are now capable of producing complete inspiral-merger-ringdown waveforms for use in injection campaigns, making it essential to validate results obtained through different numerical approaches. In this work, we used two distinct yet equally successful formulations of the Einstein equations: the modified generalized harmonic gauge and the modified CCZ4 formulation. We applied them to shift-symmetric EsGB gravity and showed that in this theory the late inspiral/merger phase evolution decelerates relative to GR, resulting in a delayed merger.

This slowing of the merger is significant because it is usually expected that in the early inspiral the phase evolution will accelerate, with a faster merger in EsGB due to additional dipolar scalar emission. Whilst we focused on a roughly equal-mass case for which the dipolar emission is suppressed, it is possible that more unequal-mass cases still show the same feature at late stages where the tensor radiation is dominant. Although our simulations do not probe sufficiently low frequencies to capture their transition from the faster to the slower inspiral regime,

we nonetheless expect such a transition to occur when the BHs are sufficiently far apart for higher order corrections to the PN approximations to be small. Longer waveforms beginning at larger separations should therefore exhibit this change in inspiral rate. If the transition were to happen within the observational band of GW detectors, it should be highly distinctive and appear in inspiral–merger–ringdown consistency tests [11–16], since it would be difficult to mimic with a change to the inferred masses. It should also be very different from the imprints of environments such as dark matter [76–79], which tend to accelerate the merger relative to GR due to increased dissipative effects (although see recent work in [80]).

We emphasize that the significance of this result is not limited to this particular theory, which as we have already noted is quite constrained by observations. It demonstrates that the common intuition that additional degrees of freedom result in a faster merger due to increased radiation of energy is not the full story, and that the effect of a modified metric and its impact on the binary dynamics can also play a significant role, particularly in the strong field regime prior to merger. A similar breakdown of the usual intuition has recently been observed in the context of oppositely charged black-hole binaries in scalar–Gauss–Bonnet theories near the scalarization threshold [81], where non-linear dynamics were found to increase eccentricity in the late inspiral, contrary to expectations that extra degrees of freedom enhance circularization. Such results underscore that non-linear strong-field dynamics can qualitatively overturn standard heuristics derived from weak-field or perturbative reasoning. They highlight the crucial role of full numerical solutions in validating modified gravity waveforms.

The next step is to define the region of the parameter space where the transition from faster to slower inspiral happens. This will depend on the mass ratio, coupling values and range of frequencies probed. Longer waveforms in the shift-symmetric theory are underway using another formulation and implementation of the Einstein equations [82, 83], which should shed more light on this effect. Injections can be used to determine how degenerate the signal is with other effects like spin-induced precession, and whether it can trigger the current tests of GR used by the LVK Collaboration, or results in a distinctive shift in the intrinsic binary parameters. There is also the exciting prospect of studying a wider range of theories, including parity violating and pure tensor theories, due to recent groundbreaking developments in well-posed formulations [84, 85]. The ultimate goal of this programme of work is to catalogue these kinds of smoking-gun effects across a range of theories, in order to discover or constrain EFT modifications using future observations. Our findings indicate that systematic cross-correlation between independent codes and complementary approximations is essential for revealing subtle phenomena that may otherwise remain undetected.

Acknowledgements.— We acknowledge helpful conversations with Sam Brady, Pau Figueras, Félix-Louis Julié, Luis Lehner, Lorenzo Pompili, Silvia Gasparotto and Jann Zosso. We thank Daniela Doneva, Will East, Peter-James Nee and Harald Pfeiffer for providing helpful comments on the manuscript. KC acknowledges support from the Simons Foundation International and the Simons Foundation through Simons Foundation grant SFI-MPS-BH-00012593-03, a UKRI Ernest Rutherford Fellowship (grant number ST/V003240/1) and an STFC Research Grant ST/X000931/1 (Astronomy at Queen Mary 2023-2026). KC and LAS thank the GRTL collaboration (www.grtlcollaboration.org) for their support and code development work. Some of the computations were performed on the Urania HPC system at the Max Planck Computing and Data Facility. This work also used the DiRAC Memory Intensive service Cosma8 at Durham University, managed by the Institute for Computational Cosmology on behalf of the STFC DiRAC HPC Facility (www.dirac.ac.uk). The DiRAC service at Durham was funded by BEIS, UKRI and STFC capital funding, Durham University and STFC operations grants. DiRAC is part of the UKRI Digital Research Infrastructure. We also used the resources and services provided by the VSC (Flemish Supercomputer Center), funded by the Research Foundation - Flanders (FWO) and the Flemish Government.

[9] D. Reitze *et al.*, Cosmic Explorer: The U.S. Contribution to Gravitational-Wave Astronomy beyond LIGO, *Bull. Am. Astron. Soc.* **51**, 035 (2019), [arXiv:1907.04833](https://arxiv.org/abs/1907.04833) [[astro-ph.IM](#)].

[10] T. Baker, D. Psaltis, and C. Skordis, Linking Tests of Gravity On All Scales: from the Strong-Field Regime to Cosmology, *Astrophys. J.* **802**, 63 (2015), [arXiv:1412.3455](https://arxiv.org/abs/1412.3455) [[astro-ph.CO](#)].

[11] B. P. Abbott *et al.* (LIGO Scientific, Virgo), Tests of General Relativity with the Binary Black Hole Signals from the LIGO-Virgo Catalog GWTC-1, *Phys. Rev. D* **100**, 104036 (2019), [arXiv:1903.04467](https://arxiv.org/abs/1903.04467) [[gr-qc](#)].

[12] R. Abbott *et al.* (LIGO Scientific, Virgo), Tests of General Relativity with Binary Black Holes from the second LIGO-Virgo Gravitational-Wave Transient Catalog, (2020), [arXiv:2010.14529](https://arxiv.org/abs/2010.14529) [[gr-qc](#)].

[13] R. Abbott *et al.* (LIGO Scientific, Virgo), Tests of general relativity with binary black holes from the second LIGO-Virgo gravitational-wave transient catalog, *Phys. Rev. D* **103**, 122002 (2021), [arXiv:2010.14529](https://arxiv.org/abs/2010.14529) [[gr-qc](#)].

[14] R. Abbott *et al.* (LIGO Scientific, VIRGO, KAGRA), Tests of General Relativity with GWTC-3, (2021), [arXiv:2112.06861](https://arxiv.org/abs/2112.06861) [[gr-qc](#)].

[15] Black Hole Spectroscopy and Tests of General Relativity with GW250114, (2025), [arXiv:2509.08099](https://arxiv.org/abs/2509.08099) [[gr-qc](#)].

[16] A. G. Abac *et al.* (LIGO Scientific, Virgo, KAGRA), GW250114: Testing Hawking’s Area Law and the Kerr Nature of Black Holes, *Phys. Rev. Lett.* **135**, 111403 (2025), [arXiv:2509.08054](https://arxiv.org/abs/2509.08054) [[gr-qc](#)].

[17] C. de Rham, S. Melville, A. J. Tolley, and S.-Y. Zhou, Positivity bounds for scalar field theories, *Phys. Rev. D* **96**, 081702 (2017), [arXiv:1702.06134](https://arxiv.org/abs/1702.06134) [[hep-th](#)].

[18] C. de Rham, A. J. Tolley, and J. Zhang, Causality Constraints on Gravitational Effective Field Theories, *Phys. Rev. Lett.* **128**, 131102 (2022), [arXiv:2112.05054](https://arxiv.org/abs/2112.05054) [[gr-qc](#)].

[19] M. Carrillo González, C. de Rham, V. Pozsgay, and A. J. J. Tolley, Causal effective field theories, *Phys. Rev. D* **106**, 105018 (2022), [arXiv:2207.03491](https://arxiv.org/abs/2207.03491) [[hep-th](#)].

[20] M. Carrillo González, C. de Rham, S. Jaitly, V. Pozsgay, and A. Tokareva, Positivity-causality competition: a road to ultimate EFT consistency constraints, *JHEP* **06**, 146, [arXiv:2307.04784](https://arxiv.org/abs/2307.04784) [[hep-th](#)].

[21] S. Weinberg, Effective Field Theory for Inflation, *Phys. Rev. D* **77**, 123541 (2008), [arXiv:0804.4291](https://arxiv.org/abs/0804.4291) [[hep-th](#)].

[22] P. Kanti, N. E. Mavromatos, J. Rizos, K. Tamvakis, and E. Winstanley, Dilatonic black holes in higher curvature string gravity, *Phys. Rev. D* **54**, 5049 (1996), [arXiv:hep-th/9511071](https://arxiv.org/abs/hep-th/9511071).

[23] T. P. Sotiriou and S.-Y. Zhou, Black hole hair in generalized scalar-tensor gravity, *Phys. Rev. Lett.* **112**, 251102 (2014), [arXiv:1312.3622](https://arxiv.org/abs/1312.3622) [[gr-qc](#)].

[24] T. P. Sotiriou and S.-Y. Zhou, Black hole hair in generalized scalar-tensor gravity: An explicit example, *Phys. Rev. D* **90**, 124063 (2014), [arXiv:1408.1698](https://arxiv.org/abs/1408.1698) [[gr-qc](#)].

[25] Z. Lyu, N. Jiang, and K. Yagi, Constraints on Einstein-dilation-Gauss-Bonnet gravity from black hole-neutron star gravitational wave events, *Phys. Rev. D* **105**, 064001 (2022), [Erratum: *Phys. Rev. D* 106, 069901 (2022)], [arXiv:2201.02543](https://arxiv.org/abs/2201.02543) [[gr-qc](#)].

[26] F.-L. Julié, L. Pompili, and A. Buonanno, Inspiral-merger-ringdown waveforms in Einstein-scalar-Gauss-Bonnet gravity within the effective-one-body formalism, *Phys. Rev. D* **111**, 024016 (2025), [arXiv:2406.13654](https://arxiv.org/abs/2406.13654) [[gr-qc](#)].

[27] E. M. Sänger *et al.*, Tests of General Relativity with

GW230529: a neutron star merging with a lower mass-gap compact object, (2024), arXiv:2406.03568 [gr-qc].

[28] H. S. Reall and C. M. Warnick, Effective field theory and classical equations of motion, *J. Math. Phys.* **63**, 042901 (2022), arXiv:2105.12028 [hep-th].

[29] Á. D. Kovács and H. S. Reall, Well-posed formulation of scalar-tensor effective field theory, *Phys. Rev. Lett.* **124**, 221101 (2020), arXiv:2003.04327 [gr-qc].

[30] Á. D. Kovács and H. S. Reall, Well-posed formulation of Lovelock and Horndeski theories, *Phys. Rev. D* **101**, 124003 (2020), arXiv:2003.08398 [gr-qc].

[31] L. Aresté Saló, K. Clough, and P. Figueras, Well-Posedness of the Four-Derivative Scalar-Tensor Theory of Gravity in Singularity Avoiding Coordinates, *Phys. Rev. Lett.* **129**, 261104 (2022), arXiv:2208.14470 [gr-qc].

[32] L. Aresté Saló, K. Clough, and P. Figueras, Puncture gauge formulation for Einstein-Gauss-Bonnet gravity and four-derivative scalar-tensor theories in $d+1$ space-time dimensions, *Phys. Rev. D* **108**, 084018 (2023), arXiv:2306.14966 [gr-qc].

[33] W. E. East and J. L. Ripley, Evolution of Einstein-scalar-Gauss-Bonnet gravity using a modified harmonic formulation, *Phys. Rev. D* **103**, 044040 (2021), arXiv:2011.03547 [gr-qc].

[34] W. E. East and J. L. Ripley, Dynamics of Spontaneous Black Hole Scalarization and Mergers in Einstein-Scalar-Gauss-Bonnet Gravity, *Phys. Rev. Lett.* **127**, 101102 (2021), arXiv:2105.08571 [gr-qc].

[35] W. E. East and F. Pretorius, Binary neutron star mergers in Einstein-scalar-Gauss-Bonnet gravity, *Phys. Rev. D* **106**, 104055 (2022), arXiv:2208.09488 [gr-qc].

[36] M. Corman, J. L. Ripley, and W. E. East, Nonlinear studies of binary black hole mergers in Einstein-scalar-Gauss-Bonnet gravity, *Phys. Rev. D* **107**, 024014 (2023), arXiv:2210.09235 [gr-qc].

[37] D. D. Doneva, L. Aresté Saló, K. Clough, P. Figueras, and S. S. Yazadjiev, Testing the limits of scalar-Gauss-Bonnet gravity through nonlinear evolutions of spin-induced scalarization, *Phys. Rev. D* **108**, 084017 (2023), arXiv:2307.06474 [gr-qc].

[38] M. Corman and W. E. East, Black hole-neutron star mergers in Einstein-scalar-Gauss-Bonnet gravity, *Phys. Rev. D* **110**, 084065 (2024), arXiv:2405.18496 [gr-qc].

[39] D. D. Doneva, L. Aresté Saló, and S. S. Yazadjiev, 3+1 nonlinear evolution of Ricci-coupled scalar-Gauss-Bonnet gravity, *Phys. Rev. D* **110**, 024040 (2024), arXiv:2404.15526 [gr-qc].

[40] F. Thaalba, N. Franchini, M. Bezares, and T. P. Sotiriou, Dynamics of spherically symmetric black holes in scalar-Gauss-Bonnet gravity with a Ricci coupling, *Phys. Rev. D* **111**, 064054 (2025), arXiv:2409.11398 [gr-qc].

[41] L. Aresté Saló, D. D. Doneva, K. Clough, P. Figueras, and S. S. Yazadjiev, Challenges in the nonlinear evolution of unequal mass binaries in scalar-Gauss-Bonnet gravity, *Phys. Rev. D* **112**, 084022 (2025), arXiv:2507.13046 [gr-qc].

[42] M. Corman, L. Lehner, W. E. East, and G. Dideron, Nonlinear studies of modifications to general relativity: Comparing different approaches, *Phys. Rev. D* **110**, 084048 (2024), arXiv:2405.15581 [gr-qc].

[43] M. Okounkova, Numerical relativity simulation of GW150914 in Einstein dilaton Gauss-Bonnet gravity, *Phys. Rev. D* **102**, 084046 (2020), arXiv:2001.03571 [gr-qc].

[44] M. Okounkova, L. C. Stein, M. A. Scheel, and D. A. Hemberger, Numerical binary black hole mergers in dynamical Chern-Simons gravity: Scalar field, *Phys. Rev. D* **96**, 044020 (2017), arXiv:1705.07924 [gr-qc].

[45] H. O. Silva, H. Witek, M. Elley, and N. Yunes, Dynamical Descalarization in Binary Black Hole Mergers, *Phys. Rev. Lett.* **127**, 031101 (2021), arXiv:2012.10436 [gr-qc].

[46] M. Elley, H. O. Silva, H. Witek, and N. Yunes, Spin-induced dynamical scalarization, descalarization, and stealthness in scalar-Gauss-Bonnet gravity during a black hole coalescence, *Phys. Rev. D* **106**, 044018 (2022), arXiv:2205.06240 [gr-qc].

[47] D. D. Doneva, A. Vañó-Viñuales, and S. S. Yazadjiev, Dynamical descalarization with a jump during a black hole merger, *Phys. Rev. D* **106**, L061502 (2022), arXiv:2204.05333 [gr-qc].

[48] T. Evstafyeva, M. Agathos, and J. L. Ripley, Measuring the ringdown scalar polarization of gravitational waves in Einstein-scalar-Gauss-Bonnet gravity, *Phys. Rev. D* **107**, 124010 (2023), arXiv:2212.11359 [gr-qc].

[49] M. Bezares, L. ter Haar, M. Crisostomi, E. Barausse, and C. Palenzuela, Kinetic screening in nonlinear stellar oscillations and gravitational collapse, *Phys. Rev. D* **104**, 044022 (2021), arXiv:2105.13992 [gr-qc].

[50] R. Cayuso, P. Figueras, T. França, and L. Lehner, Self-Consistent Modeling of Gravitational Theories beyond General Relativity, *Phys. Rev. Lett.* **131**, 111403 (2023), arXiv:2303.07246 [gr-qc].

[51] R. Cayuso and L. Lehner, Nonlinear, noniterative treatment of EFT-motivated gravity, *Phys. Rev. D* **102**, 084008 (2020), arXiv:2005.13720 [gr-qc].

[52] R. Cayuso, Gravitational collapse in quadratic gravity, *Phys. Rev. D* **108**, 124066 (2023), arXiv:2307.15163 [gr-qc].

[53] N. Franchini, M. Bezares, E. Barausse, and L. Lehner, Fixing the dynamical evolution in scalar-Gauss-Bonnet gravity, *Phys. Rev. D* **106**, 064061 (2022), arXiv:2206.00014 [gr-qc].

[54] A. H. K. R, J. L. Ripley, and N. Yunes, Where and why does Einstein-scalar-Gauss-Bonnet theory break down?, *Phys. Rev. D* **107**, 044044 (2023), arXiv:2211.08477 [gr-qc].

[55] S. E. Brady, L. Aresté Saló, K. Clough, P. Figueras, and A. P. S., Solving the initial conditions problem for modified gravity theories, *Phys. Rev. D* **108**, 104022 (2023), arXiv:2308.16791 [gr-qc].

[56] P. J. Nee, G. Lara, H. P. Pfeiffer, and N. L. Vu, Quasistationary hair for binary black hole initial data in scalar Gauss-Bonnet gravity, *Phys. Rev. D* **111**, 024061 (2025), arXiv:2406.08410 [gr-qc].

[57] B. P. Abbott *et al.* (LIGO Scientific, Virgo), Observation of Gravitational Waves from a Binary Black Hole Merger, *Phys. Rev. Lett.* **116**, 061102 (2016), arXiv:1602.03837 [gr-qc].

[58] J. L. Ripley and F. Pretorius, Scalarized Black Hole dynamics in Einstein dilaton Gauss-Bonnet Gravity, *Phys. Rev. D* **101**, 044015 (2020), arXiv:1911.11027 [gr-qc].

[59] J. L. Ripley and F. Pretorius, Gravitational collapse in Einstein dilaton-Gauss-Bonnet gravity, *Class. Quant. Grav.* **36**, 134001 (2019), arXiv:1903.07543 [gr-qc].

[60] K. Yagi, L. C. Stein, and N. Yunes, Challenging the Presence of Scalar Charge and Dipolar Radiation in Binary Pulsars, *Phys. Rev. D* **93**, 024010 (2016), arXiv:1510.02152 [gr-qc].

[61] K. Yagi, L. C. Stein, N. Yunes, and T. Tanaka, Post-Newtonian, Quasi-Circular Binary Inspirals in Quadratic Modified Gravity, *Phys. Rev. D* **85**, 064022 (2012), [Erratum: Phys. Rev. D 93, 029902 (2016)], [arXiv:1110.5950 \[gr-qc\]](https://arxiv.org/abs/1110.5950).

[62] L. Aresté Saló, S. E. Brady, K. Clough, D. Doneva, T. Evstafyeva, P. Figueras, T. França, L. Rossi, and S. Yao, GRFolres: A code for modified gravity simulations in strong gravity, *J. Open Source Softw.* **9**, 6369 (2024), [arXiv:2309.06225 \[gr-qc\]](https://arxiv.org/abs/2309.06225).

[63] T. Andrade *et al.*, GRChombo: An adaptable numerical relativity code for fundamental physics, *J. Open Source Softw.* **6**, 3703 (2021), [arXiv:2201.03458 \[gr-qc\]](https://arxiv.org/abs/2201.03458).

[64] M. Radia, U. Sperhake, A. Drew, K. Clough, P. Figueras, E. A. Lim, J. L. Ripley, J. C. Aurrekoetxea, T. França, and T. Helfer, Lessons for adaptive mesh refinement in numerical relativity, *Class. Quant. Grav.* **39**, 135006 (2022), [arXiv:2112.10567 \[gr-qc\]](https://arxiv.org/abs/2112.10567).

[65] M. Ansorg, B. Brügmann, and W. Tichy, A Single-domain spectral method for black hole puncture data, *Phys. Rev. D* **70**, 064011 (2004), [arXiv:gr-qc/0404056](https://arxiv.org/abs/gr-qc/0404056).

[66] V. Paschalidis, Z. B. Etienne, R. Gold, and S. L. Shapiro, An efficient spectral interpolation routine for the TwoPunctures code, (2013), [arXiv:1304.0457 \[gr-qc\]](https://arxiv.org/abs/1304.0457).

[67] Standalone TwoPunctures, <https://github.com/JLRiley314/Standalone-TwoPunctures-C-Cpp>.

[68] M. Okounkova, L. C. Stein, J. Moxon, M. A. Scheel, and S. A. Teukolsky, Numerical relativity simulation of GW150914 beyond general relativity, *Phys. Rev. D* **101**, 104016 (2020), [arXiv:1911.02588 \[gr-qc\]](https://arxiv.org/abs/1911.02588).

[69] B. P. Abbott *et al.* (LIGO Scientific, Virgo), Properties of the Binary Black Hole Merger GW150914, *Phys. Rev. Lett.* **116**, 241102 (2016), [arXiv:1602.03840 \[gr-qc\]](https://arxiv.org/abs/1602.03840).

[70] A. Buonanno, L. E. Kidder, A. H. Mroue, H. P. Pfeiffer, and A. Taracchini, Reducing orbital eccentricity of precessing black-hole binaries, *Phys. Rev. D* **83**, 104034 (2011), [arXiv:1012.1549 \[gr-qc\]](https://arxiv.org/abs/1012.1549).

[71] S. Habib, M. A. Scheel, and S. A. Teukolsky, Eccentricity reduction for quasicircular binary evolutions, *Phys. Rev. D* **111**, 084059 (2025), [arXiv:2410.05531 \[gr-qc\]](https://arxiv.org/abs/2410.05531).

[72] L. Lehner and O. M. Moreschi, Dealing with delicate issues in waveforms calculations, *Phys. Rev. D* **76**, 124040 (2007), [arXiv:0706.1319 \[gr-qc\]](https://arxiv.org/abs/0706.1319).

[73] C. Reisswig and D. Pollney, Notes on the integration of numerical relativity waveforms, *Class. Quant. Grav.* **28**, 195015 (2011), [arXiv:1006.1632 \[gr-qc\]](https://arxiv.org/abs/1006.1632).

[74] D. Christodoulou, Reversible and irreversible transformations in black hole physics, *Phys. Rev. Lett.* **25**, 1596 (1970).

[75] N. Sennett, S. Marsat, and A. Buonanno, Gravitational waveforms in scalar-tensor gravity at 2PN relative order, *Phys. Rev. D* **94**, 084003 (2016), [arXiv:1607.01420 \[gr-qc\]](https://arxiv.org/abs/1607.01420).

[76] J. Bamber, J. C. Aurrekoetxea, K. Clough, and P. G. Ferreira, Black hole merger simulations in wave dark matter environments, *Phys. Rev. D* **107**, 024035 (2023), [arXiv:2210.09254 \[gr-qc\]](https://arxiv.org/abs/2210.09254).

[77] J. C. Aurrekoetxea, K. Clough, J. Bamber, and P. G. Ferreira, Effect of Wave Dark Matter on Equal Mass Black Hole Mergers, *Phys. Rev. Lett.* **132**, 211401 (2024), [arXiv:2311.18156 \[gr-qc\]](https://arxiv.org/abs/2311.18156).

[78] L. Machet and L. Aresté Saló, Scalar fields from nonlinear sigma models on black hole spacetimes, *Phys. Rev. D* **112**, 084047 (2025), [arXiv:2508.18362 \[gr-qc\]](https://arxiv.org/abs/2508.18362).

[79] S. Roy, R. Vicente, J. C. Aurrekoetxea, K. Clough, and P. G. Ferreira, Scalar fields around black hole binaries in LIGO-Virgo-KAGRA, (2025), [arXiv:2510.17967 \[gr-qc\]](https://arxiv.org/abs/2510.17967).

[80] C.-H. Cheng, G. Ficarra, and H. Witek, Dephasing in binary black hole mergers surrounded by scalar wave dark matter clouds, (2025), [arXiv:2510.20037 \[gr-qc\]](https://arxiv.org/abs/2510.20037).

[81] G. Lara *et al.*, Signatures from metastable oppositely-charged black hole binaries in scalar Gauss-Bonnet gravity, (2025), [arXiv:2505.14785 \[gr-qc\]](https://arxiv.org/abs/2505.14785).

[82] G. Lara, H. P. Pfeiffer, N. A. Wittek, N. L. Vu, K. C. Nelli, A. Carpenter, G. Lovelace, M. A. Scheel, and W. Throwe, Scalarization of isolated black holes in scalar Gauss-Bonnet theory in the fixing-the-equations approach, *Phys. Rev. D* **110**, 024033 (2024), [arXiv:2403.08705 \[gr-qc\]](https://arxiv.org/abs/2403.08705).

[83] G. Lara *et al.*, (2025), (in prep).

[84] P. Figueras, A. Held, and Á. D. Kovács, Well-posed initial value formulation of general effective field theories of gravity, (2024), [arXiv:2407.08775 \[gr-qc\]](https://arxiv.org/abs/2407.08775).

[85] P. Figueras, Á. D. Kovács, and S. Yao, Stable non-linear evolution in regularised higher derivative effective field theories, *JHEP* **25**, 150, [arXiv:2505.00082 \[hep-th\]](https://arxiv.org/abs/2505.00082).

[86] A. Taracchini, Y. Pan, A. Buonanno, E. Barausse, M. Boyle, T. Chu, G. Lovelace, H. P. Pfeiffer, and M. A. Scheel, Prototype effective-one-body model for nonprecessing spinning inspiral-merger-ringdown waveforms, *Phys. Rev. D* **86**, 024011 (2012), [arXiv:1202.0790 \[gr-qc\]](https://arxiv.org/abs/1202.0790).

[87] F.-L. Julié and E. Berti, Post-Newtonian dynamics and black hole thermodynamics in Einstein-scalar-Gauss-Bonnet gravity, *Phys. Rev. D* **100**, 104061 (2019), [arXiv:1909.05258 \[gr-qc\]](https://arxiv.org/abs/1909.05258).

[88] F.-L. Julié, H. O. Silva, E. Berti, and N. Yunes, Black hole sensitivities in Einstein-scalar-Gauss-Bonnet gravity, *Phys. Rev. D* **105**, 124031 (2022), [arXiv:2202.01329 \[gr-qc\]](https://arxiv.org/abs/2202.01329).

[89] D. M. Eardley, Observable effects of a scalar gravitational field in a binary pulsar, *Astrophys. J.* **196**, 10.1086/181744 (1975).

[90] D. Sun and L. C. Stein, Parameter matching between horizon quasi-local and point-particle definitions at 1PN for quasi-circular and non spinning BBH systems in harmonic gauge, (2025), [arXiv:2510.25618 \[gr-qc\]](https://arxiv.org/abs/2510.25618).

[91] L. Lindblom and B. Szilagyi, An Improved Gauge Driver for the GH Einstein System, *Phys. Rev. D* **80**, 084019 (2009), [arXiv:0904.4873 \[gr-qc\]](https://arxiv.org/abs/0904.4873).

[92] M. W. Choptuik and F. Pretorius, Ultra Relativistic Particle Collisions, *Phys. Rev. Lett.* **104**, 111101 (2010), [arXiv:0908.1780 \[gr-qc\]](https://arxiv.org/abs/0908.1780).

[93] H. O. Kreiss and J. Oliger, Comparison of accurate methods for the integration of hyperbolic equations, *Tellus* **24**, 199 (1972).

[94] F. Pretorius, Numerical relativity using a generalized harmonic decomposition, *Class. Quant. Grav.* **22**, 425 (2005), [arXiv:gr-qc/0407110](https://arxiv.org/abs/gr-qc/0407110).

[95] M. J. Berger and J. Oliger, Adaptive Mesh Refinement for Hyperbolic Partial Differential Equations, *Journal of Computational Physics* **53**, 484 (1984).

[96] F. Pretorius and M. W. Choptuik, Adaptive mesh refinement for coupled elliptic-hyperbolic systems, *J. Comput. Phys.* **218**, 246 (2006), [arXiv:gr-qc/0508110](https://arxiv.org/abs/gr-qc/0508110).

[97] F. Pretorius, B. Stephens, and M. W. Choptuik, PAMR, <http://laplace.physics.ubc.ca/Group/Software.html>.

[98] M. Adams *et al.*, Chombo software package for AMR applications - design document, (2015).

SUPPLEMENTAL MATERIAL

Robustness of EsGB-GR Dephasing Across Formulations

In this section, we present a robustness test for the dephasing between GR and EsGB waveforms using the two independent codes employed in this work. Figure 4 shows that the dephasing between GR and EsGB waveforms within the mCCZ4 formulation is larger than the dephasing observed either between GR waveforms alone or between EsGB waveforms alone when comparing different formulations. Additionally, when we examine the difference in dephasing between EsGB and GR across the two formulations, we find that the discrepancy is significantly smaller than the differences seen when comparing GR-GR or EsGB-EsGB waveforms.

This behavior suggests, as already pointed out in Ref. [36], that the dominant truncation errors in each formulation depend only weakly on the EsGB coupling. As a result, these errors largely cancel when computing the phase difference, $\Delta\Phi$, between EsGB and GR simulations at the same resolution. Consequently, even though the individual GR and EsGB waveforms differ between the two codes, the relative dephasing between EsGB and

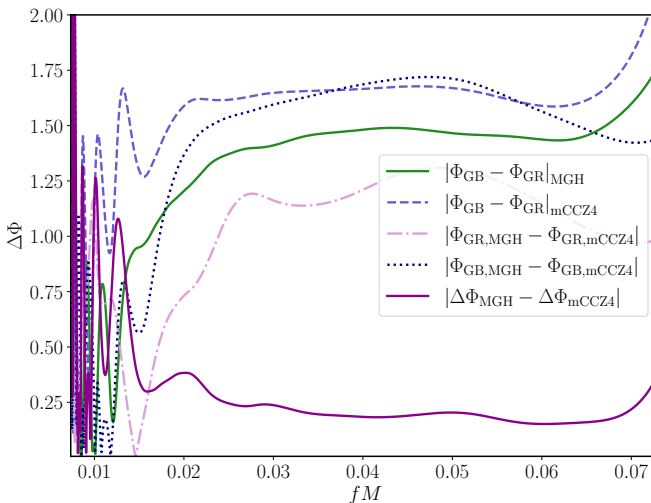


FIG. 4. Comparison plot for dephasing of waveforms after alignment in frequency and time. We show the dephasing between the two formulations for GR and EsGB individually, $|\Phi_{GR/GB, MGH} - \Phi_{GR/GB, mCCZ4}|$. We show dephasing between GR and EsGB for each formulation individually, $|\Phi_{GB} - \Phi_{GR}|_{MGH/mCCZ4}$. We also show difference in dephasing between GR and EsGB waveform between the different formulations, $|\Delta\Phi_{MGH} - \Delta\Phi_{mCCZ4}|$. This shows that even though the differences between the GR/GB phases between formulations is of the same order as the magnitude of the dephasing between EsGB and GR waveform we see in each formulation, the dephasing between GR and EsGB across codes agrees very well. The green solid and blue dashed lines are the same as those shown in Fig. 2 of the main text.

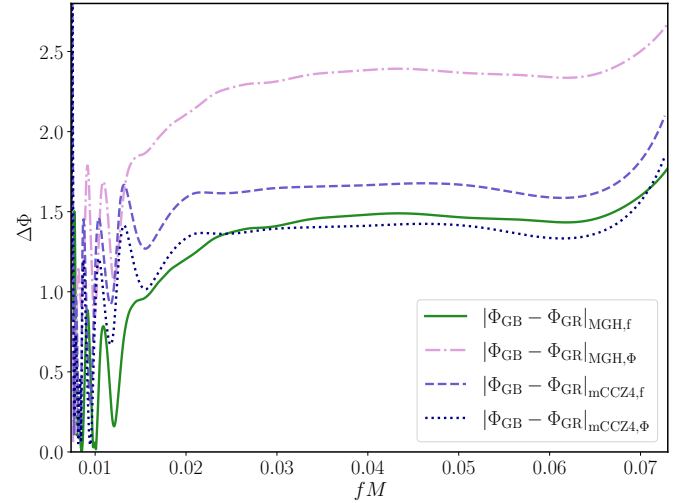


FIG. 5. Sensitivity of results on the way we perform alignment. Dephasing between GR and EsGB waveforms for each formulation after aligning the waveforms. The subscript f refers to alignment according to (4)-(5), while subscript Φ to alignment performed using (6). Note that the curves with subscript f are identical to the ones in the bottom panel of Fig. 2. We find that the results do not depend strongly on whether we align in phase only or in frequency then phase. This figure also shows agreement between the two different formulations.

GR is much more consistent across formulations.

Method of alignment

Here we explain in detail the method used for aligning the waveforms. The waveforms are aligned as was done in Ref. [26] by first minimizing the integral

$$\mathcal{I}_f(\delta t) = \int_{t_i}^{t_f} dt |f_{GR} - f_{GB}(t + \delta t)|^2, \quad (4)$$

then

$$\mathcal{I}_\Phi(\delta\Phi) = \int_{t_i}^{t_f} dt |\Phi_{GR} - \Phi_{GB}(t + \delta t) + \delta\Phi|^2, \quad (5)$$

with $\delta\Phi$ and δt being relative phase and time shifts, Φ_{GR} and Φ_{GB} denote the phases of the GR and EsGB waveforms. The alignment is done in a time window $[t_i, t_f]$ that corresponds to a low-frequency interval ($0.0074 \lesssim f_0 M \lesssim 0.0083$). The lower bound of the window should be chosen as early as possible, but late enough for junk radiation to dissipate and BHs to scalarize. We do not find that our results depend sensitively on the starting time of alignment. The upper bound is arbitrary, but should be large enough to average out numerical noise and residual eccentricity. We show in Fig. 6 that the results do not sensitively depend on the upper bound we choose.

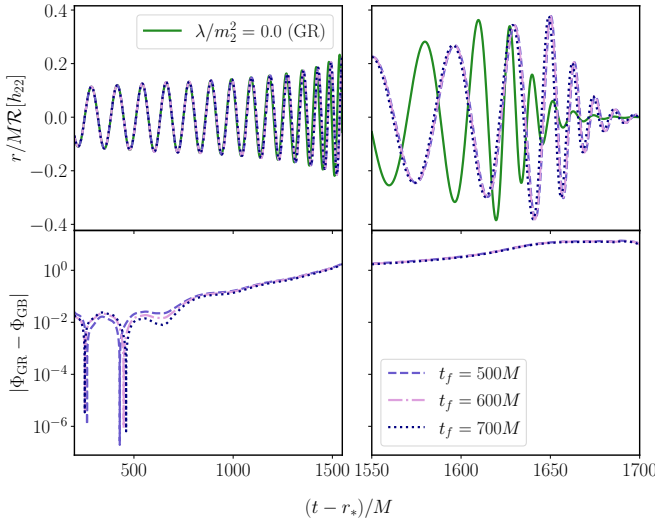


FIG. 6. Sensitivity of results on the upper bound for alignment. Top: Strain as a function of retarded time for GR (solid green) and EsGB after aligning the waveforms according to (4)-(5) with $t_i = 200M$ but varying $t_f = \{500, 600, 700\}M$. Bottom: Dephasing between GR and EsGB waveforms for the different window lengths of the top panel. We find that the alignment does not sensitively depend on the time window we choose.

We also compared to minimizing the integral

$$\mathcal{I}(\delta t, \delta\Phi) = \int_{t_i}^{t_f} dt |\Phi_{\text{GR}} - \Phi_{\text{GB}}(t + \delta t) + \delta\Phi|^2, \quad (6)$$

as was done in Ref. [86], and show in Fig. 5 that the results for both codes do not sensitively depend on the way we do the alignment.

Notion of ADM mass in numerical simulations and PN calculations

We now briefly comment on how our ADM mass compares with the PN definition, since matching these is essential for comparing PN and NR waveforms and for setting consistent NR initial data. This is mostly based on the following references [87, 88] which we refer the reader to for more details.

In GR PN theory, BHs are treated as point particles with constant masses and spins, and Einstein's equations are solved as an expansion in v/c . In EsGB, however, it is convenient to “skeletonize” the BHs in binary systems and replace the constant GR mass with a scalar-dependent function $\{m_i(\phi)\}_{i=A,B}$ determined by the value of the scalar field at the BH location [89] (with A and B referring to each one of the two BHs). Focusing on a BH in isolation first, the value of the function $m_i(\phi)$ was worked out explicitly in [87] (cf. Eq. III.8). Interestingly, a skeletonized BH was found to be fully characterized by the asymptotic scalar field value $\phi_\infty(t)$ at spatial infinity

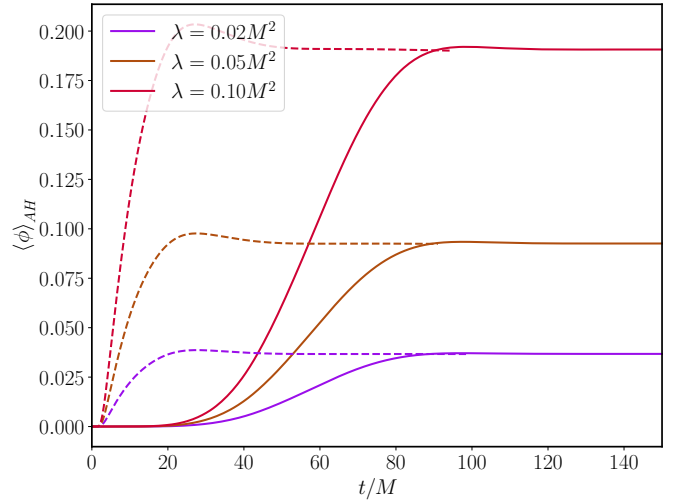


FIG. 7. Scalarization of isolated non-spinning BHs: Evolution in time of the average value of the scalar field at the Apparent Horizon for different values of the coupling constant, with dotted and solid lines corresponding to the mCCZ4 and MGH codes, respectively. Note that the scalarization takes longer in the MGH code because the coupling is slowly ramped up on a timescale of $100M$ in an analogous way as done for the BBH in this work.

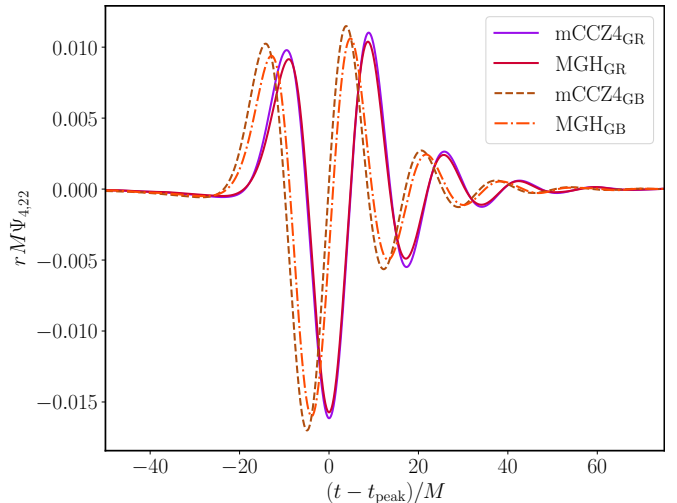


FIG. 8. Equal mass head-on mergers in EsGB and GR: Evolution in time of the (2,2) mode of the Weyl scalar extracted at spatial infinity. The differences between the two codes are compatible with truncation errors.

and its constant irreducible mass,

$$\mu_i = \sqrt{\frac{\mathcal{S}_W}{4\pi}}, \quad (7)$$

where \mathcal{S}_W is the Wald entropy (Appendix C of [87]) which reduces in shift-symmetric EsGB to [88]

$$\mathcal{S}_W = \frac{\mathcal{A}_H}{4} + 8\pi\lambda\phi_H. \quad (8)$$

This entropy satisfies the first law of thermodynamics and is the sum of the Bekenstein term and a Gauss-Bonnet contribution. The key insight of Ref. [87] was that when placing the BHs in a binary, the value of ϕ_∞ can no longer be set to zero and will depend on a far-away companion. However, when doing PN calculations, we can assume that the BHs are initially very far apart, which allows us to solve the Einstein equations not only as an expansion in v/c but also around a constant background scalar field value ϕ_0 , such that $\phi_\infty = \phi_0 + \delta\phi$, where $\delta\phi$ is at least $\mathcal{O}(1/r)$ and r is orbital separation radius. In the case of shift-symmetric EsGB, where the field equations are invariant under shifts in the scalar field, the value of ϕ_0 , which is set by the binary's cosmological environment, can be set to zero without loss of generality. Finally, the masses of BHs that enter all PN expressions for the potential, fluxes and waveforms are the $m_i(\mu_i, \phi_0) \equiv m_i^0$ (see e.g Eq.(IV.6) in [87]).

We computed the Wald entropy of each BH in our simulations and found that it changes by only $\sim 0.6, 0.3\%$ for the smaller and bigger BH during scalarization, respectively, and remains nearly constant thereafter. Using these entropies, we evaluated $m_i^0(\mu_i, \phi_0)$ from Eq. (III.8) of [87] (with $\phi_0 = 0$) for each BH and obtained a total mass of $M^0 \equiv m_A^0 + m_B^0$, which differs only by $\sim 0.2\%$ from the total initial ADM mass of the spacetime. Similarly we find that the mass ratio between EsGB and GR waveforms differs by 0.007%. These differences are not sufficient to significantly change the dephasing we see and so we do not pursue mass-definition ambiguities further, although this remains a subtle issue even in GR (see [90]).

Expected dephasing in PN theory

It is useful to show what PN theory predicts the dephasing to be for the system we study. The gravitational modes $h_{\ell m}$ have been computed to 2PN (relative to the quadrupolar radiation in GR) and we refer to Ref. [26] for complete expressions or Section III.D of Ref. [38] for a summary of the PN predictions. Substituting the intrinsic parameters of the system we study, the top panel of Fig. 9 shows the expected phase evolution up to 2PN as a function frequency all the way up to merger for both the EsGB and GR waveforms. Note that at any given frequency $\Phi_{\text{GB}}(f) > \Phi_{\text{GR}}(f)$ which is in direct contradiction to the results found in this letter (cf. Fig. 2). We also show the dephasing in the middle panel which again disagrees with what we found. Note however that even though the PN approximations predict that the EsGB system should inspiral faster than GR at any given frequency all the way up to near merger, this effect diminishes at high frequencies. Moreover, we find that the highest PN corrections, namely 1.5 and 2PN, reduce the rate of inspiral with respect to GR, which was already observed in Ref. [38]. Finally we also compare the quantity $d\Phi/df \sim (df/dt)^{-1}$

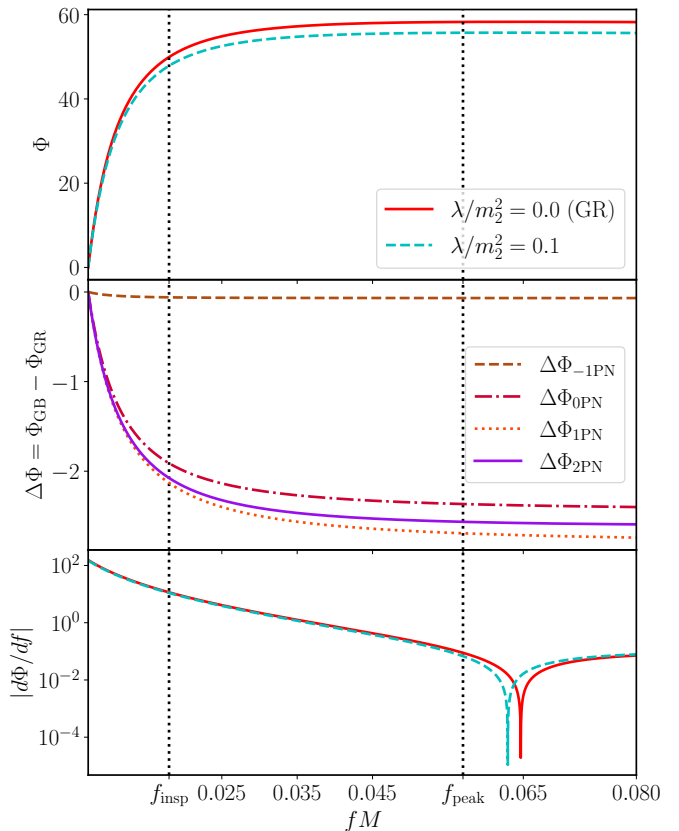


FIG. 9. PN predictions for the phase in EsGB and GR using same intrinsic parameters and range of frequencies probed by system studied in this paper. Top: Phase as a function of frequency in both GR (solid) and EsGB (dashed) gravity. We note that the behaviour is the opposite to that observed in Fig. 2. Middle: Dephasing between EsGB and GR waveform as a function of frequency up to 2PN, where again even the most accurate approximation is in disagreement with our results. We also show the dephasing when only considering leading order (dipolar) contribution to phase and all contributions up to 0PN and 1PN order. Bottom: The quantity $d\Phi/df \sim (df/dt)^{-1}$ as a function of frequency for GR and EsGB. The first vertical line corresponds to the end of inspiral stage in GR $f_{\text{insp}} = 0.018M$, and the second to frequency at which amplitude of GR waveform peaks f_{peak} . The smaller value for EsGB implies a faster inspiral.

at any given frequency, which is larger in GR, again supporting the idea that the EsGB waveform inspirals faster when compared to GR.

Code comparison

In this section we provide a detailed description of the two independent numerical implementations used in this work, the MGH and mCCZ4 formulations, for evolving the full, non-perturbative, shift-symmetric EsGB equations. In both formulations, one introduces two auxiliary Lorentzian metrics \tilde{g}^{mn} and \hat{g}^{mn} that obey certain causal-

ity conditions. Adopting a gauge in these formulations amounts to choosing the functional form of the auxiliary metrics, as well as the functional form of the source function H^c . There is significant freedom in choosing the auxiliary metrics as functions of the physical metric g_{ab} , but as in Refs. [31, 33] we choose $\tilde{g}^{ab} = g^{ab} - \tilde{A}n^a n^b$ and $\hat{g}^{ab} = g^{ab} - \hat{A}n^a n^b$, where n^a is the (timelike) unit vector orthogonal to the spacelike hypersurfaces we evolve on, and \tilde{A} and \hat{A} are constants set to 0.2 and 0.4, respectively. However, the two approaches differ in the choice of source function. The MGH formulation uses the modified version of the damped harmonic gauge, sometimes fixed in time to maintain Kerr-Schild like coordinates [91, 92]. The mCCZ4 scheme, on the other hand, employs a generalized moving-puncture gauge based on 1+log slicing and Gamma-driver conditions. Both methods discretize the evolution equations with fourth-order Runge–Kutta time integration and fourth finite-difference stencils, supplemented by Kreiss–Oliger dissipation [93] and constraint damping. The MGH formulation directly evolves the covariant system, inverting the resulting linear equations at each grid point using Gaussian elimination, and employs compactified coordinates, as detailed in Ref. [94], so that physical boundary conditions (namely that the metric is flat and the scalar field vanishes) can be placed at spatial infinity. In contrast, the mCCZ4 formulation uses a finite Cartesian grid with standard Sommerfeld boundaries and a 3+1 conformal decomposition of the equations. Both utilize Berger-Oliger [95] style adaptive mesh refinement (AMR), implemented via the PAMR [96, 97] and Chombo [98] libraries, respectively with third-order temporal interpolation for the AMR boundaries. Treatment of BHs also differs: the MGH approach relies on dynamic excision of regions within apparent horizons, with second-order extrapolation to repopulate grid points as horizons evolve, while the mCCZ4 scheme uses the moving-puncture technique to avoid explicit excision and smoothly suppresses the higher-derivative terms inside horizons. Further implementation details can be found in the respective references.

Here we show additional results, complementary to the quasi-circular BBH studied in the main body of the manuscript, which helped us validate our codes.

We first focus on the scalarization of isolated non-spinning BHs for different coupling parameters λ , ranging from $\lambda/M^2 = 0.02$ to 0.1. Figure 7 shows the evolution in time of the average value of the scalar field on the BH apparent horizons, $\langle \phi \rangle_{\text{AH}}$, for three different values of the coupling constant, with dotted and solid lines corresponding to the mCCZ4 and MGH codes, respectively, with excellent agreement in the values attained after scalarization.

We then study equal mass head-on collisions with an initial separation of $50M$ for $\lambda/M^2 = 0.025$, and compare

the gravitational radiation to GR. Figure 8 displays the (2,2) mode of the Weyl scalar for both GR and EsGB, showing very good agreement between the two codes. We have shifted the waveforms in time so that both MGH and mCCZ4 codes merge at $t = 0$ in GR and we have kept the same negative dephasing between GR and EsGB present in the raw data. Given that head-on mergers have no phase evolution, there is no notion of frequency and so there is no obvious way to align GR and non-GR waveforms. Since the initial transients induce a change of the velocities with which the punctures are moving towards each other, the GR and EsGB waveforms may represent different physical systems. However, this does not change the main message of Figure 8, which is the agreement of our codes for both GR and beyond GR head-on mergers.

Comparison to previous works

Finally, we comment on why the effects presented in this letter were not visible in our earlier works, in particular [36] and [41], despite these studies using the same versions of our codes. In the MGH simulations of [36], no eccentricity-reduction procedure was applied, and the EsGB waveforms were slightly more eccentric than their GR counterparts due to initial transients caused by BH scalarization. The available waveforms were also too short to allow an alignment over the longer time interval used here—an interval that is crucial for averaging out numerical noise and residual eccentricity. In the mCCZ4 runs of [41], the waveform alignment between the GR and EsGB waveforms was also not done using the robust method used here, and the value of the coupling studied was lower. In the unequal mass cases the presence of a larger amount of dipole radiation may also have reduced the effect, and although the eccentricity was similar between the GR and EsGB cases, the fact that the orbits were non-circular will have changed the dynamics and reduced the ability to robustly align them. By contrast, the waveforms employed in the present study are substantially longer, have undergone eccentricity reduction, and therefore permit a robust alignment procedure. This improved setup was essential for enabling the rigorous code comparison that ultimately made the findings of this letter apparent.

Note that hints of this effect have already appeared in fully non-linear, quasi-circular, and eccentricity-reduced simulations of black hole–neutron star mergers in Einstein–scalar–Gauss–Bonnet gravity using the MGH formulation [38]. In that work, even though the neutron star does not carry scalar charge and scalar radiation is therefore expected to be non-negligible, it was found that the additional dephasing beyond the inspiral stage is negligible (see Fig. 3 of Ref. [38]).